Spatial distributions of upper tropospheric water vapor measurements from the UARS Microwave Limb Sounder

Elizabeth M. Stone[1,2], Liwen Pan[3], Brad J. Sandor[3], William G. Read[1], and Joe W. Waters[1]

Short title: SPATIAL DISTRIBUTIONS OF MLS WATER VAPOR

[1]Jet Propulsion Laboratory, California Institute of Technology, Pasadena, CA

[3]National Center for Atmospheric Research, Boulder, CO

[2]Now at Bay Area Environmental Research Institute, NASA Ames Research Center, Moffett Field, CA

Abstract. We characterize measurements of upper tropospheric (~300–150 hPa) water vapor obtained from the Microwave Limb Sounder (MLS) instrument on board the Upper Atmosphere Research Satellite (UARS) in terms of their spatial and temporal variability. We present the climatology of water vapor mixing ratio for October 1991–June 1997, which includes the seasonal means, the root-mean-square deviations, and the seasonal differences. The climatology of the divergent wind field is compiled to examine the relationship of upper tropospheric moisture fields and the tropical circulations. The spatial climatological features found in the water vapor data appear consistent with known tropospheric circulations. The tropical wet and dry patterns are latitudinally distributed in accordance with the Hadley circulation and longitudinal distributions correspond well to the Walker circulation.

We quantify the frequency of dry tropical observations in seasonal maps. The most prominent dry regions are located in the subtropics and associated with the downward motions of the Hadley cell. On the 316 hPa surface there is some occurrence of low values of humidity throughout the majority of the tropics, while at 215 hPa, it is primarily the subsidence regions that show dry values. Subtropical dry observations are more frequent in the Southern Hemisphere winter than in the Northern Hemisphere winter.

The seasonal cycle of MLS water vapor is compared with Stratospheric Aerosol and Gas Experiment II (SAGE II) measurements. Good agreement is found between these two data sets for measurements near the extratropical tropopause and the data are consistent with the known seasonal cycle of water vapor in the lowermost stratosphere. Potential vorticity analysis is used to indicate whether extratropical measurements were influenced primarily by stratospheric or tropospheric air. Frequency distributions display distinct characteristics and seasonal dependence for these two regions.

1. Introduction

Water vapor plays an essential role in atmospheric processes through its radiative, chemical, and dynamical properties. In the upper troposphere, it is one of the key greenhouse gases which absorbs longwave terrestrial radiation and its distribution is strongly influenced by both the large-scale circulation and localized convection. Chemically, water vapor is a major source of the hydroxyl radical, the primary oxidant in the troposphere which is able to react with most pollutants. The role of the radiative feedback mechanisms of water vapor in global warming scenarios has undergone considerable study (e.g. *Lindzen* [1990]; *Rind et al.* [1991]; *Houghton et al.* [1996]; *Yang and Tung* [1998]; *Inamdar and Ramanathan* [1998]). Rising surface temperatures may cause greater evaporation and increased water vapor amounts and thus enhance the absorption of outgoing radiation. However, it has been suggested that increasing convective activity could act to dry the upper troposphere through the detrainment of dry air from convective towers. Also central to the relationship between water vapor and the earth's climate is the extent of the dry, large-scale subsidence regions, where more outgoing longwave radiation is lost to space, and the degree to which these regions offset increasing greenhouse warming (*Pierrehumbert* [1995]). Thus, the understanding of global water vapor distributions is crucial for climate prediction which incorporates the positive and/or negative radiative feedback mechanisms of water vapor.

Water vapor is also a valuable tracer of atmospheric motions (e.g. *Rodgers et al.* [1976]; *Appenzeller and Norton* [1996]) and its transport represents movement of energy in the form of latent heat. Recent studies of transport across the tropical tropopause have brought attention to water vapor distributions and their budgets in the lower stratosphere and upper troposphere (e.g. *Mote et al.* [1998]; *Dessler* [1998]). Other studies utilize measurements of water vapor and focus on the mechanisms and evidence for transport across the extratropical tropopause (*Hintsa et al.* [1998]; *Dessler et al.* [1995]). Analyses of the seasonal cycles and hemispheric asymmetries in extratropical water vapor in the lowermost stratosphere have also been used to study the details of transport in these regions (*Rosenlof et al.* [1997]; *Pan et al.* [1997]).

One data set available for the study of water vapor in the upper troposphere is from the Microwave Limb Sounder (MLS) instrument (*Barath et al.* [1993]) on board the Upper Atmosphere Research Satellite. This data set in its preliminary form was first reported on by *Read et al.* [1995] and the version used in this analysis, v4.90, is validated by *Read et al.* (manuscript in preparation, 1999).

The purpose of this study is to examine the observed spatial characteristics of this data set in relation to tropospheric circulation and transport issues. This is an extension of the analysis of the zonal mean seasonal behavior of the MLS upper tropospheric humidity (UTH) by *Sandor et al.* [1998]. Our analyses focus on the spatial distributions of the water vapor and their relation to the Hadley and Walker circulations. In the tropics, these circulations largely control the moisture patterns. We present the seasonal distributions of the frequency of dry measurements in the tropical upper troposphere. The prominent dry regions are associated with the locations of tropical subsidence. We also examine the water vapor seasonal cycle near the extratropical tropopause, a region influenced by stratosphere-troposphere exchange. Although the MLS data product examined here is named "upper tropospheric" water vapor, the pressure levels on which the data are available can be located above the extratropical tropopause. Thus the data set contains values for water vapor in the upper troposphere and lowermost stratosphere. Comparison with measurements from the Stratospheric Aerosol and Gas Experiment II (SAGE II), which primarily samples the lower stratosphere, is presented to establish a consistent picture of water vapor in the middleworld.

2. Data

The MLS measurement technique is described by *Waters* [1993], the UARS instrument by *Barath et al.* [1993], and a summary of results from UARS MLS is given by *Waters et al.* [1999]. MLS began taking measurements, approximately 1300 profiles each day, in September 1991 and operated continuously for three years, after which the instrument made intermittent measurements. Our study covers measurements made during the September 1991–

June 1997 time period. Latitudinal coverage by the instrument is from 80° in one hemisphere to 34° in the other hemisphere, alternating approximately every 36 days with the satellite yaw maneuvers. The MLS UTH data are retrieved and reported in units of relative humidity with respect to ice (RH_i) and converted to mixing ratio units (ppmv) with National Centers for Environmental Prediction (NCEP) analysis temperatures. A detailed description of the MLS UTH data product and its retrieval is provided by *Read et al.* (manuscript in preparation, 1999). Version 4.90 of the data, used here, is improved over the preliminary version (*Read et al.* [1995]) by utilizing an improved empirical expression for dry and wet continuum emission and by accounting for field-of-view and refractive effects. The UTH data are retrieved on four pressure levels, 464, 316, 215, 147 hPa. As noted earlier, these pressure levels can be located above the extratropical tropopause. The discussion in this paper will focus on the upper three surfaces and will include data for the upper troposphere and lowermost stratosphere. As described by *Read et al.* (manuscript in preparation, 1999), the measurement resolution is limited by the vertical retrieval points (2.7 km) when the atmosphere is dry (below 30% RH_i). For higher humidities, the resolution degrades to ~4 km (the correlation length of the a priori profile) beginning with the lowest altitude retrieval coefficient and proceeding upwards as the atmosphere moistens. The resolution of the upper two levels (147 hPa and 215 hPa) is not degraded until the atmosphere becomes wetter than 90%. When interpreting these data, it should be noted that the measurement resolution can be coarser than the horizontal and vertical gradients of water vapor. One strength of these measurements is the ability of MLS to measure in the presence of cirrus clouds. In addition, its temporal resolution is better than that of solar occultation measurements of water vapor and its vertical resolution is finer than that of the nadir-looking infrared operational sounders.

A detailed validation of the MLS UTH data product and the improvements made since the initial version is reported by *Read et al.* (manuscript in preparation, 1999). The validation compares the MLS UTH with coincident data from other humidity measurement techniques including frost point hygrometers and Vaisala sondes (corrected for cold temperatures).

Reporting comparisons relative to these measurements, the MLS UTH at 147 hPa is on average 25% wetter than the coincident frost point hygrometer measurements and 12% drier than the cold temperature corrected Vaisala sonde data. At 215 hPa, the MLS data is 9% and 50% drier compared with the frost point hygrometers and cold temperature corrected Vaisala sondes, respectively. The 316 hPa and 464 hPa levels tend to have a severe dry bias when the atmosphere is wet, in part due to retrieval problems. An empirical data quality screening method, recommended by *Read et al.* (manuscript in preparation, 1999), eliminates many of the badly retrieved points and was used on the data presented here. With the recommended screening, the MLS UTH at 464 hPa and 316 hPa is 13% and 32% drier than the cold temperature corrected Vaisala sondes. The data quality screening technique rejects more low latitude measurements than high latitude measurements which results in a less uniform sampling over the tropics for the lower two levels.

3. Water Vapor Climatological Features

3.1. Spatial Distributions of Water Vapor and Divergent Wind

Figure 1 presents the MLS upper tropospheric water vapor mixing ratio seasonal means on the 215 hPa level. These maps were formed by averaging the measurements made for each season in 10° longitude by 5° latitude bins. Measurements where retrieved relative humidity exceeds 100% (due to cloud emissions) are set to 100% to improve the humidity accuracy. The relative humidity value is then converted to volume mixing ratio (ppmv) using the same NCEP temperatures used by the retrieval. The fraction of measurements that exceed 100% RH_i is strongly dependent on latitude and altitude. At 10S-10N and 147 hPa, a region of high relative humidity, *Jensen et al.* [1999] report 28% of measurements exceed 100% RH_i. On the drier 215 hPa pressure surface shown in Figure 1, only 12% of measurements exceed 100% for 10S-10N, and 7% of measurements are saturated for 30S-30N. The figure shows considerable variability in the water vapor fields in latitude and longitude along with seasonal changes.

Sandor et al. [1998] discuss the zonal mean analysis of the annual cycles in the data set. The deviation from the zonal mean values can be large, particularly in the Northern Hemisphere (NH) summer season, so that the spatial distribution of water vapor presents information not present in the zonal mean picture. A thorough discussion of atmospheric circulations and their impact on cloud occurrence and water vapor distributions over the eastern Pacific and North America can be found in *Haas and Pfister* [1998]. A discussion of the annual and intraseasonal variability in the MLS water vapor data at 215 hPa is given by *Clark et al.* [1998].

Seasonal mean water vapor mixing ratios in the upper troposphere are largest in the tropics near the equator (Figure 1). In this region the tropical Hadley cell and convective systems provide strong vertical transport of water vapor. The tropical maximum in Figure 1 moves across the equator following the summer season and the shifting of the intertropical convergence zone (ITCZ). The largest seasonally-averaged mixing ratios on this pressure surface, with values exceeding 200 ppmv, are found in the vicinity of the Southeast Asian/Indian monsoon (15°N–20°N latitude and 70°–100°E longitude) in the June through August months (JJA). In addition to the high mixing ratios in the ITCZ and monsoon areas, other tropical wet regions are found over the Southern Hemisphere (SH) land masses, Central America, and in the South Pacific Convergence Zone (SPCZ). There is a large gradient to the north and west of the Asian monsoon region, with much lower values at 30°N–50°N and 0°–90°E longitude.

Tropical tropospheric circulations consist of several closed cells in the zonal-vertical plane. The dominant east-west cell, known as the Walker circulation, is found in the equatorial Pacific and exhibits rising motions in the western Pacific and descent over the eastern Pacific. The velocity potential and divergent wind fields are useful in identifying the vertical motions of the Walker circulation and tropical regions of upwelling and subsidence (*Newell et al.* [1996]). *Newell et al.* [1996] analyzed the Walker circulation for two time segments during the Pacific Exploratory Mission West (PEMW) campaign. Their results describe the rising and sinking branches of the Walker cell and show a good agreement between the MLS UTH and

the divergent wind fields.

We extend the work of *Newell et al.* [1996] by examining the global climatology of the divergent wind and the MLS water vapor fields for all four seasons. This highlights the impact of the longitudinally asymmetric circulations on the water vapor distributions. Seasonal means of the upper tropospheric water vapor overlaid with contours of velocity potential and divergent wind vectors are presented in Figure 2. Monthly mean velocity potential fields at 200 hPa from the NCEP Reanalysis project (*Kalnay et al.* [1996]), are seasonally averaged for the October 1991–June 1997 time segment used in this study.

The climatology of the divergent winds shows two major tropical regions of upper level divergence, indicating outflow and rising air from below. The largest is found in the western Pacific. In DJF, this divergence region is located between 5S°–10°S and is centered over Indonesia. It extends from 70°E, over the Indian Ocean to the central Pacific. By MAM, the eastern portion of this feature has shifted northward by about 5° while the line of divergence over the Indian ocean has shifted to the south. In JJA, the divergence region is centered near 15°N, coinciding with the Asian monsoon, and extends from the western to the central Pacific. The velocity potential values are much larger in JJA compared to the other seasons. The second major divergence region occurs over South and Central America. It is positioned over the South American continent in DJF and is shifted northward in MAM. By JJA, the divergence is near Central America. A weaker region of divergence is found over the north central Pacific in DJF and MAM. Convergence, indicating descent or subsidence is found over the eastern Pacific, off the coast of South America throughout the year. In the NH summer and fall seasons, the convergence extends northward across the equator, depicting the mid Pacific trough. In DJF and MAM, there is a line of convergence extending across the Atlantic ocean near 20°N. Convergence also exists at 30°S, 0°E–90°E and over North Africa in the seasons from March through November, and across Asia in DJF. The features shown in the divergent wind climatology agree well with the east-west circulations described by *Krishnamurti* [1971] and with the analysis for PEMW by *Newell et al.* [1996].

Figure 2 shows mixing ratios consistent with the spatial distribution of the divergent wind field and the east-west tropical circulations. Divergence coincides with moist regions in the western Pacific, along the ITCZ, and over the tropical land masses. Convergence is aligned with local minima in mixing ratio and drier tropical locations. This indicates that the longitudinal distribution of tropical upper tropospheric water vapor is largely controlled by the circulation cells in the zonal-vertical plane.

Water vapor mixing ratio values tend to decrease away from the equator. However, tropical features of high mixing ratio values are seen to extend into the midlatitudes, particularly in the summer seasons. In the NH summer months, tropical features extend to ~50°N over the western to central Pacific and off the east coast of North America. Seasonal mixing ratios in this region have maximum values that range from 75 ppmv to 160 ppmv. *Hu and Liu* [1998] show that these moist regions in the extratropics coincide with enhanced convective cloud amount due to baroclinic activity. In DJF in the SH, wet regions extend out of the tropics to 40°S primarily over the oceans. The driest seasonal values are found in the NH winter, to the north and west of the seasonal jet core maximum and major winter storm track regions. The SH extratropical fields display a comparatively more zonally-symmetric field throughout the year.

3.2. Spatial Distributions of Seasonal Differences

Other features in the water vapor climatology can be highlighted by examining the difference between the water vapor distributions in the DJF and JJA seasons (Figure 3). This difference gives an indication of the fluctuation of water vapor due to seasonal changes. In particular, we examine the longitudinal locations of seasonal change as evidenced in the zonally asymmetric distributions of seasonal differences. On the three upper tropospheric levels available in the MLS data set, the seasonal mean mixing ratios are generally higher in the summer hemisphere at all latitudes. The exceptions to this are found at high latitudes in both hemispheres, off the coast of South America, and Northwest of the Asian monsoon

region. For latitudes poleward of ~50° at 147 hPa and to a lesser extent for the high latitudes at 215 hPa, the winter values exceed the summer values. These regions are primarily in the stratosphere and mixing ratios are generally less than the systematic sensitivity of the measurement. Off the west coast of South America from the Equator to 40°S, the JJA mean mixing ratios are slightly larger or nearly identical to those in DJF on the 215 hPa and 147 hPa surfaces. This area is influenced by the downward arm of the Walker circulation and as shown by *Clark et al.* [1998], the annual variation here is small. The dry values found to the northwest of the Asian monsoon in JJA, noted in Figure 1, result in a slightly drier summertime in this region compared to winter values. The Kyzlkum desert (near 40°N, 65°E) and strong localized descent is found within this dry feature. A model study of the monsoon-desert mechanism in this region showed the descent of midlatitude air to be remotely forced (*Rodwell and Hoskins* [1996]). The dry values are found at all four levels of the MLS UTH data set and they produce a strong semi-annual component to the time series for the region in contrast to the prominent annual cycle seen in the zonal mean values of the subtropics (*Sandor et al.* [1998]). Off the west coast of North America (centered at 30°N, 230°E), the seasonal variations are very small at 215 hPa and positive (indicating a slightly wetter winter than summer) for the 316 hPa and 147 hPa levels. As described in *Haas and Pfister* [1998], the summertime dryness in this region is due to downward motion associated with the mid-Pacific trough.

The largest seasonal variations at all three pressure levels occur in the NH over India and SE Asia. At 215 hPa, the differences exceed 150 ppmv. From 30°N–45°N over the Southeast Asia and the Western Pacific, DJF mixing ratios are over 90% less than the values in this region for the JJA season. Other large NH variations are found over Central America, and near the east coast of the US. SH seasonal variations are less than those found in the NH. The largest seasonal variations in the SH are confined to 10°S–20°S on all three pressure levels. The location of these differences coincides with the three main convective centers over the land masses, and an area in the central Pacific. At 215 hPa the largest variations in the SH exceed 100 ppmv and JJA values are 70% less than those in the DJF season.

At the core of the seasonal differences in the tropics is the seasonal shift in the position of the Hadley circulation (*Del Genio et al.* [1994]; *Sun and Oort* [1995]). Figure 3 shows that outside the tropics, the MLS water vapor shows significant seasonal variations in the NH which are zonally-asymmetric and with maxima spatially located over eastern North America and the western Pacific. Seasonal differences in the extratropical SH are smaller in magnitude than those found in the NH. General circulation model analyses by *Del Genio et al.* [1994] found that it is the large-scale eddy moisture fluxes which act to increase the summer upper tropospheric humidity values in the extratropics.

3.3. Intraseasonal Variability

The root-mean-square (rms) deviation about the seasonal or monthly means in the MLS upper tropospheric water vapor gives an indication of the temporal variability contained in this data set. This variability encompasses the atmospheric variability as well as any inherent to the instrument noise and sampling. The MLS measurement noise for UTH is negligible compared to the atmospheric variability. One reason for assessing the rms deviation of measurements of atmospheric water vapor is for comparison with climate models to test their ability to capture reasonable variability in their convective schemes (*Soden and Bretherton* [1994]). The analysis by *Peixoto and Oort* [1996] of the climatology of radiosonde relative humidity measurements, showed the maximum day to day rms deviation in that data to be in the midlatitudes with lower variability in the tropics from the surface to 300 hPa. Winter variability was found to be somewhat higher than summer above the boundary layer. From 500–300 hPa, there was a secondary maximum in the rms deviation of the relative humidity measurements at 10° latitude in the summer hemisphere. Zonal mean rms deviations of January and July mean total precipitable water from SSM/I show maximum variability between 30°–60° latitude due to the impact of transient eddies in this region and minimum variability over the tropical and subtropical regions (*Soden and Bretherton* [1994]).

Figure 4 presents the temporal rms deviation about the DJF and JJA seasonal means

shown in Figure 1. The contours of rms deviation resemble those of the mean value, suggesting a somewhat linear relationship between the two fields. The largest variability occurs in JJA over the monsoon region, where rms deviations are between 80–120 ppmv and mean values are 200–220 ppmv.

In order to examine the latitudinal dependence in the mean and rms deviation, Figure 5 plots the zonal mean mixing ratios in January and July along with the rms deviation of those means for the three pressure levels. The zonal mean values peak in the tropics, shifted from the equator towards the summer hemisphere, and decrease toward the poles. At 147 hPa, both winter poles show an increase in the zonal mean mixing ratios (and rms deviations). From the middle to high latitudes, the zonal mean values and rms deviations are nearly identical at 215 and 147 hPa. The extratropical data at 316 hPa show rms deviations lower than the mean value in the summer hemisphere and nearly identical in the winter. In the tropics, the amount of variability relative to the zonal mean value decreases with altitude. At the 147 hPa level, the tropical rms deviations are constant with latitude and peak at $\pm 30°$ in both January and July. The 215 hPa and 316 hPa data also show a peak in the rms deviations at 30°N in July.

3.4. Distribution of Dry Tropical Observations

In this section we quantify and examine the spatial distribution of the frequency of dry tropical observations in the upper tropospheric water vapor. We define dry values as those in which the relative humidity is less than 10%. Figure 6 shows the seasonal percentage of occurrence of these dry events in 10° longitude by 5° latitude bins over the globe for the 316 hPa and 215 hPa pressure surfaces. Measurements considered to be above the extratropical tropopause (defined by absolute values of potential vorticity larger than 3 PVU, where 1 PVU = 10^{-6} m^2 K s^{-1} kg^{-1}) are excluded from the analysis. On the 147 hPa surface (not shown), the occurrences of relative humidity values of less than 10% are found primarily poleward from the boundaries of the tropics. Equatorward of $\pm 15°$ latitude there are almost no measurements with values less than 10% at 147 hPa (see Figure 1 in *Jensen et al.* [1999]).

The spatial distributions of dry tropical measurements shown in the seasonal maps quantify the magnitude and extent of the dry regions. The maps depict the regionality and seasonality of the tropical subsidence regions for the 316 hPa and 215 hPa levels. The dry air occurrences show large zonal asymmetries and hemispheric differences. The largest number of dry air observations is found in the subtropics of the winter hemisphere, consistent with the dominance of the Hadley cell in the winter hemisphere. In the DJF season, dry observations occur primarily over the Atlantic (290°E–310°E longitude) and Pacific oceans (70°E–210°E longitude) centered near 20°N. The dry feature over the Pacific extends westward across southeast Asia and India to the African continent. The Pacific shows a higher percentage of dry observations than the Atlantic in this season. Dry tropical observations in JJA are most prominent in the eastern half of the SH from 15°S–30°S. A second dry region is seen from 0°S–20°S in the vicinity of 240°E. At 215 hPa the eastern Pacific dry observations are less frequent than what is found from 0°E–180°E. As discussed earlier, there is a region of dry observations in the NH in the JJA season to the northwest of the Asian monsoon. Also present in the NH summer season is evidence of dryness to the east of the mid-Pacific trough. The spatial distributions of dry regions presented in Figure 6 are consistent with the maps of relative humidities from SSM/I for January and July 1994 (*Spencer and Braswell* [1997]).

The driest regions have relative humidity values of less than 10% in roughly 70% of the observations. The two pressure levels show different features in the percentages of dry tropical observations. At 316 hPa the majority of the area in the tropics contains instances of low relative humidity while at 215 hPa it is only the subsidence regions that show occurrences of dry values. The frequency of relative humidity values less than 10% for all observations between 30°N-30°S at 316 hPa is 30% (40%) in DJF (JJA). At 215 hPa, the occurrence frequency of dry values is below 20% in this latitude band. Also shown in Figure 6 is a hemispheric asymmetry in the distribution of subtropical dry regions. A higher percentage of dry observations is found in the SH in JJA than in the NH DJF.

4. Water Vapor Near the Extratropical Tropopause

4.1. Seasonal Cycles and Comparison With SAGE II Data

To compliment the spatial climatology of the MLS water vapor discussed in Section 3, we next present a zonal picture of the water vapor seasonal cycle and quantify the tropical and extratropical monthly means and hemispheric differences. In the extratropics, the MLS water vapor measurement samples the troposphere and lowermost stratosphere. Potential vorticity based zonal means can be used to calculate the water vapor seasonal cycle for dynamically similar air masses. We also make a comparison of the MLS seasonal cycle in potential vorticity coordinates with that from SAGE II measurements.

Figure 7 shows the area weighted monthly mean and annual average of tropical (0°–35° latitude) and extratropical (35°–65° latitude) mixing ratios for each hemisphere. For the 316 hPa and 215 hPa pressure levels, the tropical annual cycles peak in June and July in the NH and in February–March in the SH. NH tropical monthly means are greater than or equal to the SH means for the equivalent month of the year throughout the annual cycle. The annual average in the NH exceeds that of the SH by 60 ppmv at 316 hPa and 10 ppmv at 215 hPa. The hemispheric differences in the tropical annual and monthly averages at 147 hPa are much smaller than systematic uncertainties in the data and may not be significant.

The maximum extratropical monthly mean mixing ratio in the NH occurs in July (300 ppmv at 316 hPa and 50 ppmv at 215 hPa). In the SH, the annual cycle peaks in February (210 ppmv at 316 hPa and 30 ppmv at 215 hPa). For the 316 hPa and 215 hPa levels, the annual cycle of NH extratropical water vapor shows larger mixing ratios than those of the SH in the summer months and near equivalent values in the winter and spring seasons. During the summer months the SH extratropical means are 60% to 75% of those in the NH for equivalent months. The annual extratropical average is ~20 ppmv larger in the NH than in the SH at 316 hPa and the hemispheres differ by less than 5 ppmv at the 215 hPa level. Most of this difference comes from wetter summer months in NH. Some caution should be exercised

because the difference is comparable to systematic uncertainties in the data. At 147 hPa, where extratropical data are often above the tropopause, mixing ratios values are small and generally less than the systematic sensitivity of the measurement at this level (10 ppmv).

Care should be taken in interpreting these annual cycles. The pressure levels on which the MLS upper tropospheric water vapor product is retrieved, can, at times, be located in the lower stratosphere in the extratropics. Thus, embedded in the monthly mean values in Figure 7 is the change with season of the tropopause pressure. Also, the vertical resolution and range of sensitivity of the MLS measurements can limit the information in the data above the extratropical tropopause.

In order to separate the seasonal variation of tropopause height from the variability in the water vapor for the MLS measurements in the vicinity of the extratropical tropopause, we compile the annual cycle of the water vapor in potential vorticity–potential temperature (PV–θ) coordinates and make a comparison to those from the SAGE II experiment. SAGE II (*McCormick* [1987]) is a solar occultation instrument which measures water vapor with a $\sim$1 km vertical resolution from the cloud tops to 50 km in altitude. The instrument obtains 15 sunrise and 15 sunset profiles each day. This sampling results in a much finer vertical resolution but less daily horizontal coverage than that of MLS. The SAGE II data examined in this comparison were compiled for the five years 1986–1990. We group both sets of data into monthly mean PV–θ bins with widths of 1 PVU and 10 K. The PV–θ coordinate ensures that, within the limitations of the instruments' resolution, the mean values are comprised of dynamically similar air parcels. The range of PV–θ values in this comparison span the vicinity of the extratropical tropopause and lowermost stratosphere.

The two data sets show qualitative agreement in the annual cycles for PV values from 1–6 PVU and potential temperatures from 310 K–350 K. The MLS values tend to be larger during the summer seasons, particularly at the lower potential temperature surfaces. This could be attributed in part to the coarser vertical resolution of the MLS data. Because water vapor mixing ratios decrease exponentially with altitude, the width of the measurements will

cause values to be biased toward the lower, wetter altitudes. The PV–θ bins in this comparison are outside of the tropics where clouds would interfere significantly with the SAGE II measurements. A representative example of the annual cycles of the MLS and SAGE II water vapor for two different PV–θ bins in each hemisphere is shown in Figure 8. Also seen in the figure is a larger rms deviation in the MLS water vapor monthly means compared to those of SAGE II. While the MLS measurements are not as sensitive to low mixing ratios (less than $\sim$10 ppmv) and stratospheric values of water vapor, the agreement in the annual cycles shown in Figure 8 supports the usefulness of the MLS data in extratropical studies near the tropopause.

Measurements of water vapor near the extratropical tropopause and the study of the seasonal cycles and hemispheric differences in water vapor data have been used to help understand transport characteristics in the lowermost stratosphere and the mechanisms which control the seasonal cycles in this region (e.g. *Dessler et al.* [1995]; *Hintsa et al.* [1998]; *Pan et al.* [1997]; *Rosenlof et al.* [1997]). While these mechanisms are qualitatively understood, how each process contributes quantitatively to the water vapor budget is less known. The analysis presented here supports the previously established seasonal cycle of water vapor in the lowermost stratosphere. The magnitude of the monthly mean values are significantly larger than mixing ratios representative of water vapor in the overworld. Thus, the seasonal cycles in Figure 8 suggest a significant contribution of transport from the troposphere to the lowermost stratosphere. The summer seasons, in particular the NH summer, shows evidence of more effective transport from the troposphere.

4.2. Frequency Distributions

We further examine the information contained in the extratropical water vapor from MLS by focusing on frequency distributions of the measurements. In doing this we look for distinct characteristics which identify and separate measurements of tropospheric and stratospheric air. In addition, the frequency distributions give information not present in the climatological

means in that they display the range of values for this portion of the atmosphere. As previously noted, the vertical resolution of the UTH measurement may result in measurements which span the transition between the troposphere and the stratosphere and the values will reflect a perhaps significant influence of moister air below the tropopause. We use PV analysis to indicate whether the measured values were influenced primarily by tropospheric or stratospheric air. The extratropical data at 215 hPa are separated according to PV criteria where PV < 2 PVU indicates tropospheric observations and $3 <$ PV ≤ 6 PVU defines values at or above the extratropical tropopause. Figure 9 presents the normalized frequency distributions for the water vapor measurements separated by these criteria. The distributions are limited to the 35°–60° latitude ranges in the winter and summer seasons. These results are not sensitive to small changes in the PV criteria used. We focus on the 215 hPa level since it provides a significant number of points in both PV bins. At 147 hPa there is only a small number of midlatitude measurements which coincide with PV values less than 2 PVU.

Figure 9 shows that the criteria used to isolate the tropospheric and stratospheric measurements result in two distinctive frequency distributions with seasonal variations. The tropospheric data display a broader frequency distribution and peak at a higher mixing ratio than that of the stratospheric data for both the summer and winter seasons, indicating that the extratropical troposphere is moister and more variable than the lowermost stratosphere. The overlap of the two distributions is smallest in the summer season of each hemisphere. The frequency distribution for all the extratropical data most resembles that of the $3 <$ PV ≤ 6 PVU criteria in the winter seasons. The wintertime extratropical data for this pressure level consist largely of stratospheric measurements while in the summer there is roughly an equal number of measurements for the two regions marked by the PV ranges. This is consistent with the lower altitude of the extratropical tropopause in the winter seasons. The frequency distributions of both PV criteria peak at higher mixing ratios in the summer than in the winter seasons of both hemispheres. In addition, both frequency distribution curves are broadest in the summer months (followed by fall and spring; winter months have the narrowest distributions).

Interpretation of the broadness of the frequency distributions is complicated by the vertical resolution of the MLS measurement. However, the broadness and higher mode values of the summertime distributions for the $3 < PV \leq 6$ PVU range suggests that transport across the extratropical tropopause is prominent during this season. This is in agreement with the seasonal variability of water vapor in the lowermost stratosphere discussed by *Pan et al.* [1999]. The distributions for the two hemispheres differ in that the NH summer distributions peak at a higher mixing ratio than for the SH. These frequency distributions reinforce the seasonal cycle analysis and the hemispheric asymmetries noted in the previous section. They are also consistent with an interpretation of a summer maximum in transport into the lowermost stratosphere.

5. Summary

Results presented in this paper illustrate the spatial patterns and climatological features in the global MLS upper tropospheric water vapor data. The seasonal means, rms deviations, and seasonal differences were analyzed for this data set. Climatological means were shown to be consistent with the seasonal movement of the ITCZ and tropical circulations. Tropical wet and dry regions coincide with divergence and convergence identified in the climatology of the divergent wind fields. In this way, the zonally-asymmetric features in the water vapor are in agreement with the east-west Walker circulation.

Seasonal maps of the frequency of dry observations in the upper troposphere quantify the extent of the dry regions. The dominant dry regions depict subsidence associated with the Hadley and Walker circulations. The spatial distributions of the dry observations are zonally asymmetric. Dry regions in the SH show a higher percentage of observations of low relative humidity values than the NH. At 316 hPa relative humidity values less than 10% are observed throughout the tropics, with an occurrence frequency of 30%-40% for $\pm 30^\circ$ latitude. At 215 hPa it is primarily the subsidence regions that are dry.

We examined the extratropical water vapor data by comparing the seasonal cycles with

those from SAGE II and by examining the frequency distributions of measurements, grouped by PV analysis, to indicate data representative of tropospheric air from those which are influenced by stratospheric air. Qualitative agreement is found in the seasonal cycles of MLS and SAGE II near the extratropical tropopause and lowermost stratosphere. The quantitative differences, most evident in the wettest months, are likely due to the very different sampling of the two instruments. The MLS climatology supports existence of a pronounced seasonal cycle of water vapor in this region previously established by analysis of aircraft and satellite measurements. Although for low mixing ratios the MLS UTH measurements are not sensitive to variations on the order of a few ppmv, the annual cycle analysis provides evidence that the data contains valuable information in the extratropics near the tropopause and lowermost stratosphere. However, in order to discern variability that is smaller than the estimated systematic error of the measurements and atmospheric variability, it is necessary to use the MLS UTH data set in a statistical or average sense rather than isolating individual profiles.

Acknowledgments. The analysis in this paper was performed while E. M. Stone held a National Research Council post-doctoral associateship at the California Institute of Technology, Jet Propulsion Laboratory. Work by others at JPL was done under contract with the National Aeronautics and Space Administration. We acknowledge the members of the MLS team for their work in producing the UTH data product.

References

Appenzeller, C. H., and W. A. Norton, Fragmentation of stratospheric intrusions, *J. Geophys. Res.*, *101*, 1435–1456, 1996.

Barath, F. T., et al., The Upper Atmosphere Research Satellite Microwave Limb Sounder instrument, *J. Geophys. Res.*, *98*, 10,751–10,762, 1993.

Clark, H. L., R. S. Harwood, P. W. Mote, and W. G. Read, Variability of water vapor in the tropical upper troposphere as measured by the Microwave Limb Sounder on UARS, *J. Geophys. Res.*, *103*, 31,695–31,707, 1998.

Del Genio, A. D., W. Kovari Jr., and M.-S. Yao, Climatic implications of the seasonal variation of upper troposphere water vapor, *Geophys. Res. Lett.*, *21*, 2701–2704, 1994.

Dessler, A. E., A reexamination of the "stratospheric fountain" hypothesis, *Geophys. Res. Lett.*, *25*, 4165–4168, 1998.

Dessler, A. E., E. J. Hintsa, E. M. Weinstock, J. G. Anderson, and K. R. Chan, Mechanisms controlling water vapor in the lower stratosphere: "A tale of two stratospheres", *J. Geophys. Res.*, *100*, 23,167–23,172, 1995.

Haas, M. R., and L. Pfister, A high-altitude site survey for SOFIA, *Publications of the Astronomical Society of the Pacific*, *110*, 339–364, 1998.

Hintsa, E. J., et al., Troposphere-to-stratosphere transport in the lowermost stratosphere from measurements of H_2O, CO_2, N_2O and O_3, *Geophys. Res. Lett.*, *25*, 2655–2658, 1998.

Houghton, J. T., L. G. M. Filho, B. A. Callander, N. Harris, A. Kattenber, and K. Maskell, eds., *Climate Change 1995: The Science of Climate Change*, Cambridge University Press, New York, 1996.

Hu, H., and W. T. Liu, The impact of upper tropospheric humidity from Microwave Limb Sounder on the midlatitude greenhouse effect, *Geophys. Res. Lett.*, *25*, 3151–3154, 1998.

Inamdar, A. K., and V. Ramanathan, Tropical and global scale interactions among water vapor, atmospheric greenhouse effect, and surface temperatures, *J. Geophys. Res.*, *103*, 32177–32194, 1998.

Jensen, E. J., W. G. Read, J. Mergenthaler, B. J. Sandor, L. Pfister, and A. Tabazadeh, High humidities and subvisible cirrus near the tropical tropopause, *Geophys. Res. Lett.*, *26*, 2347–2350, 1999.

Kalnay, E., et al., The NCEP/NCAR 40-year reanalysis project, *Bull. Amer. Meteor. Soc.*, *77*, 437–471, 1996.

Krishnamurti, T. N., Observational study of the tropical upper tropospheric motion field during the Northern Hemisphere summer, *J. App. Meteor.*, *10*, 1066–1096, 1971.

Lindzen, R. S., Some coolness concerning global warming, *Bull. Amer. Meteor. Soc.*, *71*, 288–299, 1990.

McCormick, M. P., SAGE II: An overview, *Adv. Space Res.*, *7(3)*, 219–226, 1987.

Mote, P. W., T. J. Dunkerton, M. E. McIntyre, E. A. Ray, P. H. Haynes, and J. M. Russell III, Vertical velocity, vertical diffusion, and dilution by midlatitude air in the tropical lower stratosphere, *J. Geophys. Res.*, *103*, 8651–8666, 1998.

Newell, R. E., Y. Zhu, E. V. Browell, W. G. Read, and J. W. Waters, Walker circulation and tropical upper tropospheric water vapor, *J. Geophys. Res.*, *101*, 1961–1974, 1996.

Pan, L., S. Solomon, W. Randel, J.-F. Lamarque, P. Hess, J. Gille, E.-W. Chiou, and P. M. McCormick, Hemispheric asymmetries and seasonal variations of the lowermost stratospheric water vapor and ozone derived from SAGE II data, *J. Geophys. Res.*, *102*, 28,177 – 28,184, 1997.

Pan, L., E. J. Hintsa, E. M. Stone, E. M. Weinstock, and W. Randel, The seasonal cycle of water vapor and saaturation mixing ratio in the lowermost stratosphere, *J. Geophys. Res.*, 1999, under review.

Peixoto, J. P., and A. H. Oort, The climatology of relative humidity in the atmosphere, *J. Climate*, *9*, 3443–3463, 1996.

Pierrehumbert, R. T., Thermostats, radiator fins, and the local runaway greenhouse, *J. Atmos. Sci.*, *52*, 1784–1806, 1995.

Read, W. G., J. W. Waters, D. A. Flower, L. Froidevaux, R. F. Jarnot, D. L. Hartmann, R. S. Harwood, and R. B. Rood, Upper-tropospheric water vapor from *UARS* MLS, *Bull. Amer. Meteor. Soc.*, *76*, 2381–2389, 1995.

Rind, D., E.-W. Chiou, W. Chu, J. Larsen, S. Oltmans, J. Lerner, M. P. McCormick, and L. McMaster, Positive water vapour feedback in climate models confirmed by satellite data, *Nature*, *349*, 500 – 503, 1991.

Rodgers, E. B., V. V. Salomonson, and H. L. Kyle, Upper tropospheric dynamics as reflected in Nimbus 4 THIR 6.7-μm data, *J. Geophys. Res.*, *81*, 5749–5758, 1976.

Rodwell, M. J., and B. J. Hoskins, Monsoons and the dynamics of deserts, *Q. J. R. Meteorol. Soc.*, *122*, 1385–1404, 1996.

Rosenlof, K. H., A. F. Tuck, K. K. Kelly, J. M. Russell III, and M. P. McCormick, Hemispheric asymmetries in water vapor and inferences about transport in the lower stratosphere, *J. Geophys. Res.*, *102*, 13,213–13,234, 1997.

Sandor, B. J., W. G. Read, J. W. Waters, and K. H. Rosenlof, Seasonal behavior of tropical to midlatitude upper tropospheric water vapor from UARS MLS, *J. Geophys. Res.*, *103*, 25,935 – 25,947, 1998.

Soden, B. J., and F. P. Bretherton, Evaluation of water vapor distribution in general circulation models using satellite observations, *J. Geophys. Res.*, *99*, 1187–1210, 1994.

Spencer, R. W., and W. D. Braswell, How dry is the tropical free troposphere? Implications for global warming theory, *Bull. Amer. Meteor. Soc.*, *78*, 1097–1106, 1997.

Sun, D.-Z., and A. H. Oort, Humidity-temperature relationships in the tropical troposphere, *J. Climate*, *8*, 1974–1987, 1995.

Waters, J. W., Microwave limb sounding, in *Atmospheric Remote Sensing by Microwave Radiometry*, edited by M. A. Janssen, pp. 383–496, John Wiley, New York, 1993.

Waters, J. W., et al., The UARS and EOS Microwave Limb Sounder (MLS) experiments, *J. Atmos. Sci.*, *56*, 194–218, 1999.

Yang, H., and K. K. Tung, Water vapor, surface temperature, and the greenhous effect– a statistical analysis of tropical-mean data, *J. Climate*, *11*, 2686–2697, 1998.

Elizabeth M. Stone, NASA Ames Research Center, Mail Stop 245-4, Moffett Field, CA, 94035

William G. Read, Elizabeth M. Stone, and Joe W. Waters, Jet Propulsion Laboratory, 4800 Oak Grove Drive, MS 183-701, Pasadena, CA, 91109-8099

Liwen Pan and Brad J. Sandor, National Center for Atmospheric Research, P. O. Box 3000 Boulder, CO 80307-3000

Submitted to *J. Geophys. Res.*,

Figure Captions

Figure 1. Seasonal averages of MLS upper tropospheric water vapor on the 215 hPa surface. Color contours are of 2, 5, 10, 20, 50, 100, 200 ppmv.

Figure 2. Seasonal averages of MLS upper tropospheric water vapor on the 215 hPa surface (in color) overlaid with contours of velocity potential (in increments of 200×10^4 m^2 s^{-1}) and divergent wind vectors (with a maximum amplitude of 7.6 m s^{-1}).

Figure 3. Seasonal differences (DJF - JJA) for MLS upper tropospheric water vapor on the 215 hPa surface. Contours are of 0, ±30., ±60., ... ppmv.

Figure 4. The rms deviation about monthly mean MLS upper tropospheric water vapor on the 215 hPa surface for DJF and JJA. Color contours refer to color bar in Figure 1.

Figure 5. The rms deviation (dashed line) and monthly mean zonal mean (solid line) MLS upper tropospheric water vapor for January (blue) and July (red).

Figure 6. Percentages of the MLS observations on the 215 hPa (top) and 316 hPa (bottom) surfaces in which relative humidity values are less than 10%. Contours are from 10% to 90% incremented by 10%.

Figure 7. Monthly mean values of MLS upper tropospheric water vapor on the 147, 215, and 316 hPa surfaces. Filled symbols indicate tropical (0°–30° latitude) averages; open symbols indicate extratropical averages (35°–65°). Red (blue) symbols are for SH (NH) data. Dashed lines show the annual averages.

Figure 8. Monthly mean water vapor mixing ratio and rms deviation from MLS (circles) and SAGE II (squares). Data are binned by PV–θ values. Bins sizes are 1 PVU and 10 K. SH means are shown on the left; NH means are on the right.

Figure 9. Normalized frequency distributions for midlatitude (35° - 60° latitude) water vapor mixing ratio in the NH and SH for DJF and JJA. Distributions are formed for data with PV < 2 PVU (red), $3 <$ PV ≤ 6 PVU (blue), and all data (black). The number of data points in the distributions is listed in the upper right hand corner each panel.

Figures

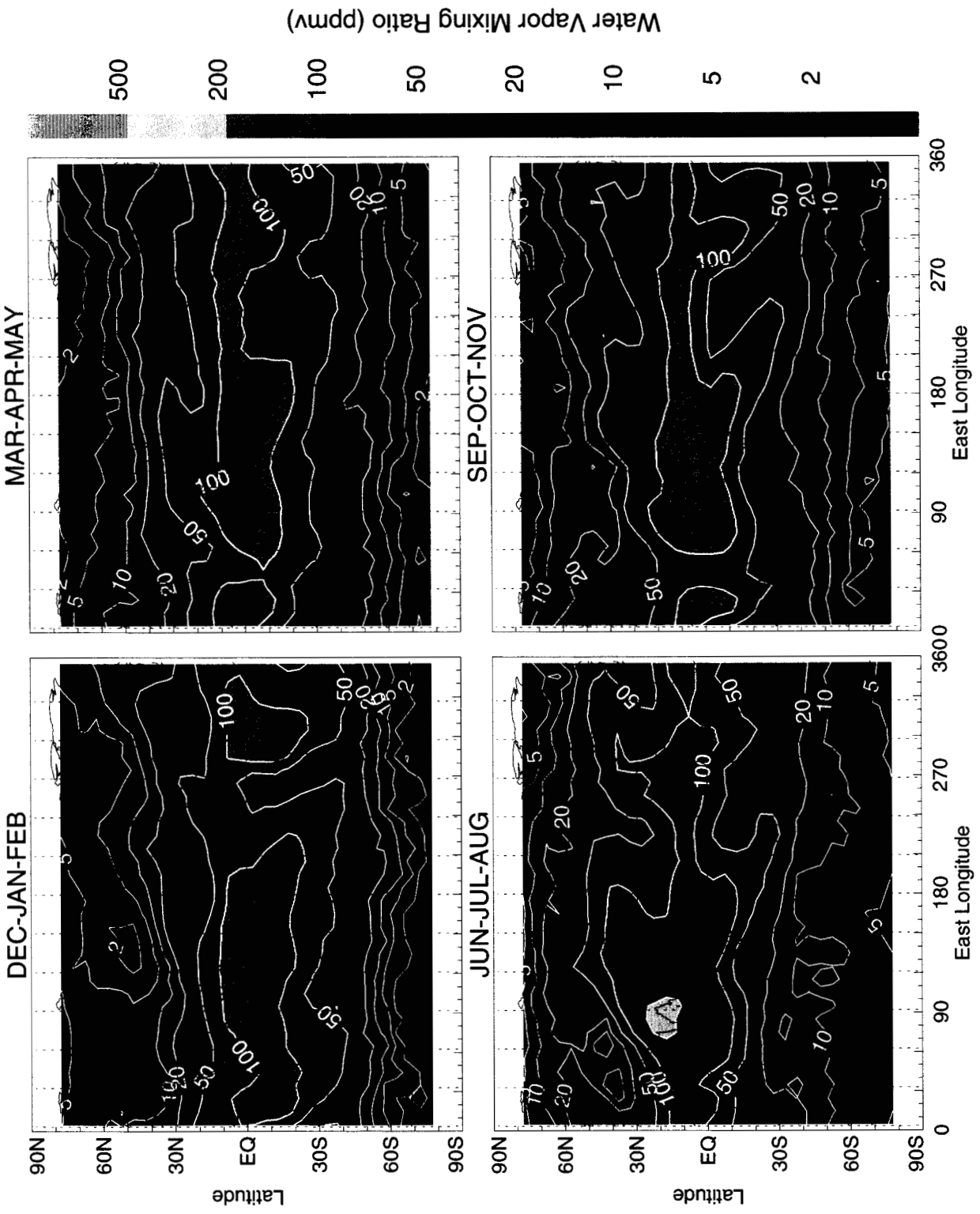

Figure 1. Seasonal averages of MLS upper tropospheric water vapor on the 215 hPa surface. Color contours are of 2, 5, 10, 20, 50, 100, 200 ppmv.

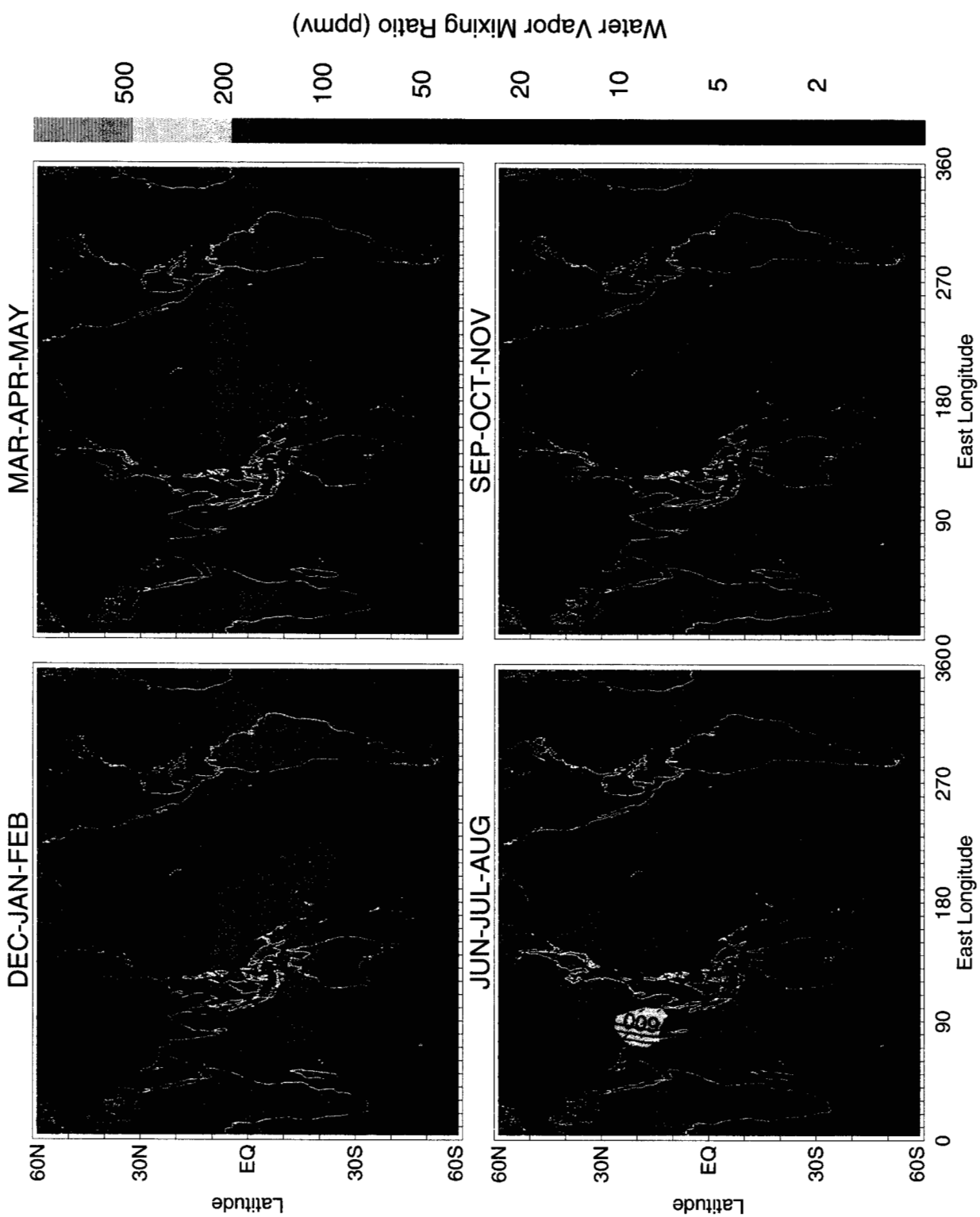

Figure 2. Seasonal averages of MLS upper tropospheric water vapor on the 215 hPa surface (in color) overlaid with contours of velocity potential (in increments of 200×10^4 m^2 s^{-1}) and divergent wind vectors (with a maximum amplitude of 7.6 m s^{-1}).

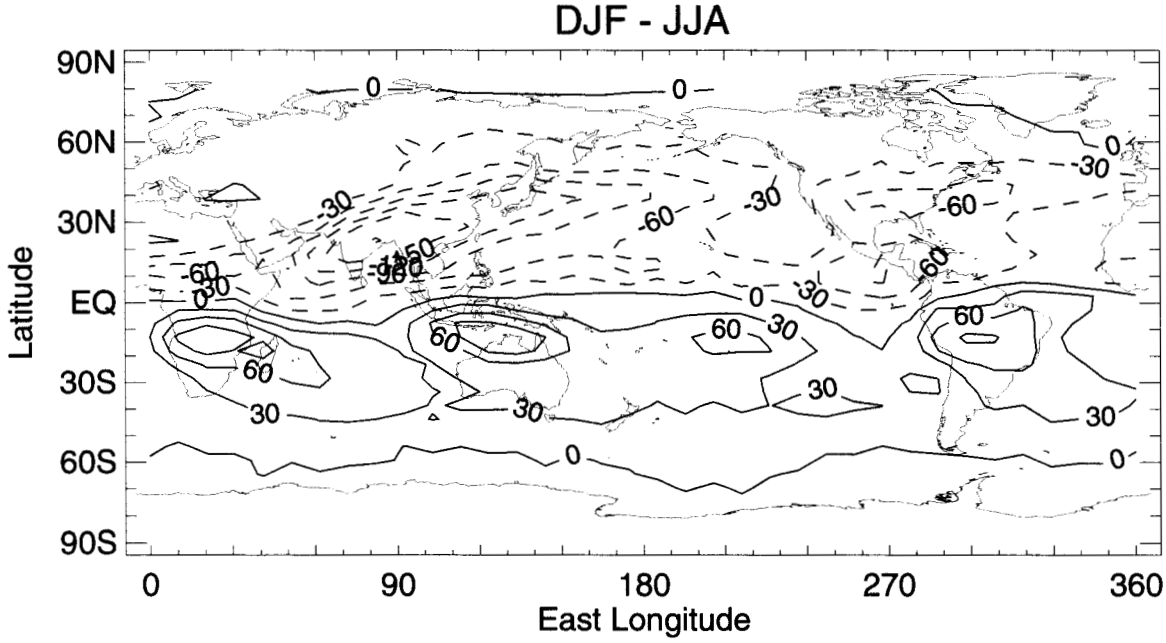

Figure 3. Seasonal differences (DJF - JJA) for MLS upper tropospheric water vapor on the 215 hPa surface. Contours are of 0, ±30., ±60., ... ppmv.

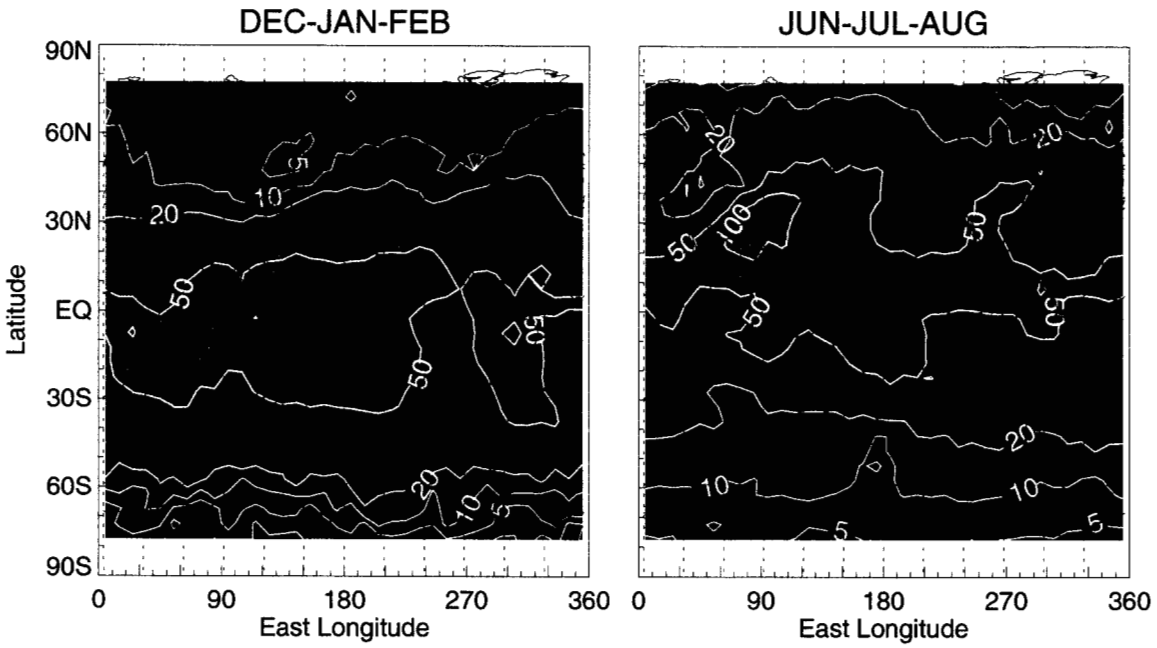

Figure 4. The rms deviation about monthly mean MLS upper tropospheric water vapor on the 215 hPa surface for DJF and JJA. Color contours refer to color bar in Figure 1.

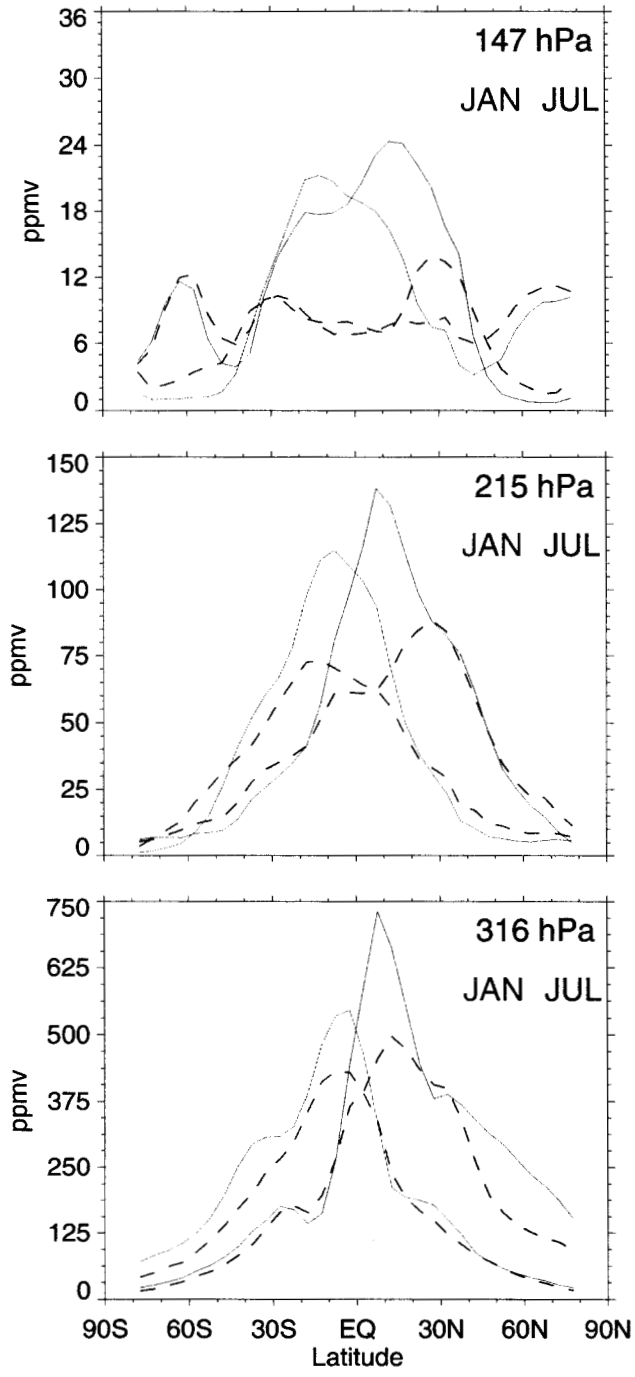

Figure 5. The rms deviation (dashed line) and monthly mean zonal mean (solid line) MLS upper tropospheric water vapor for January (blue) and July (red).

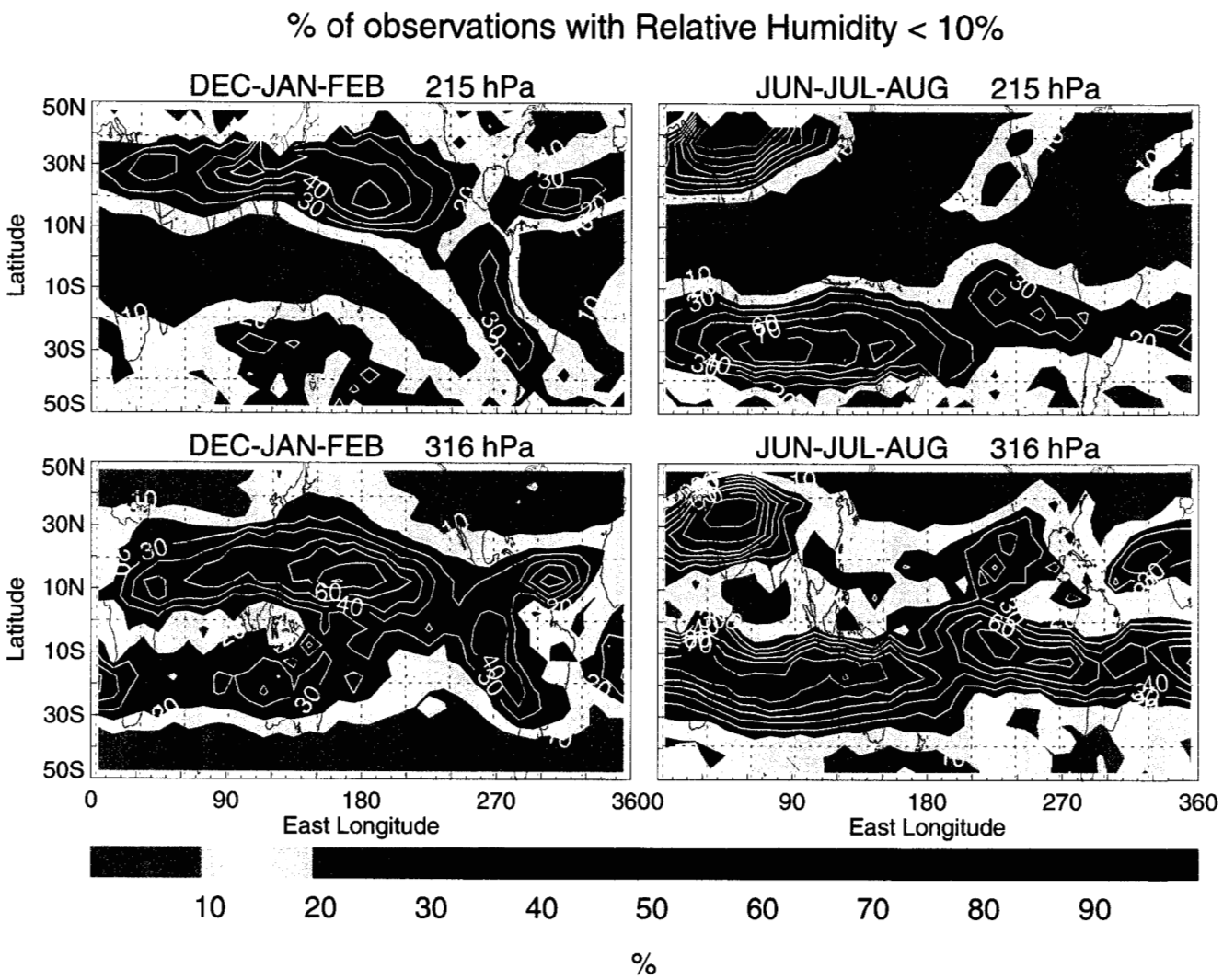

Figure 6. Percentages of the MLS observations on the 215 hPa (top) and 316 hPa (bottom) surfaces in which relative humidity values are less than 10%. Contours are from 10% to 90% incremented by 10%.

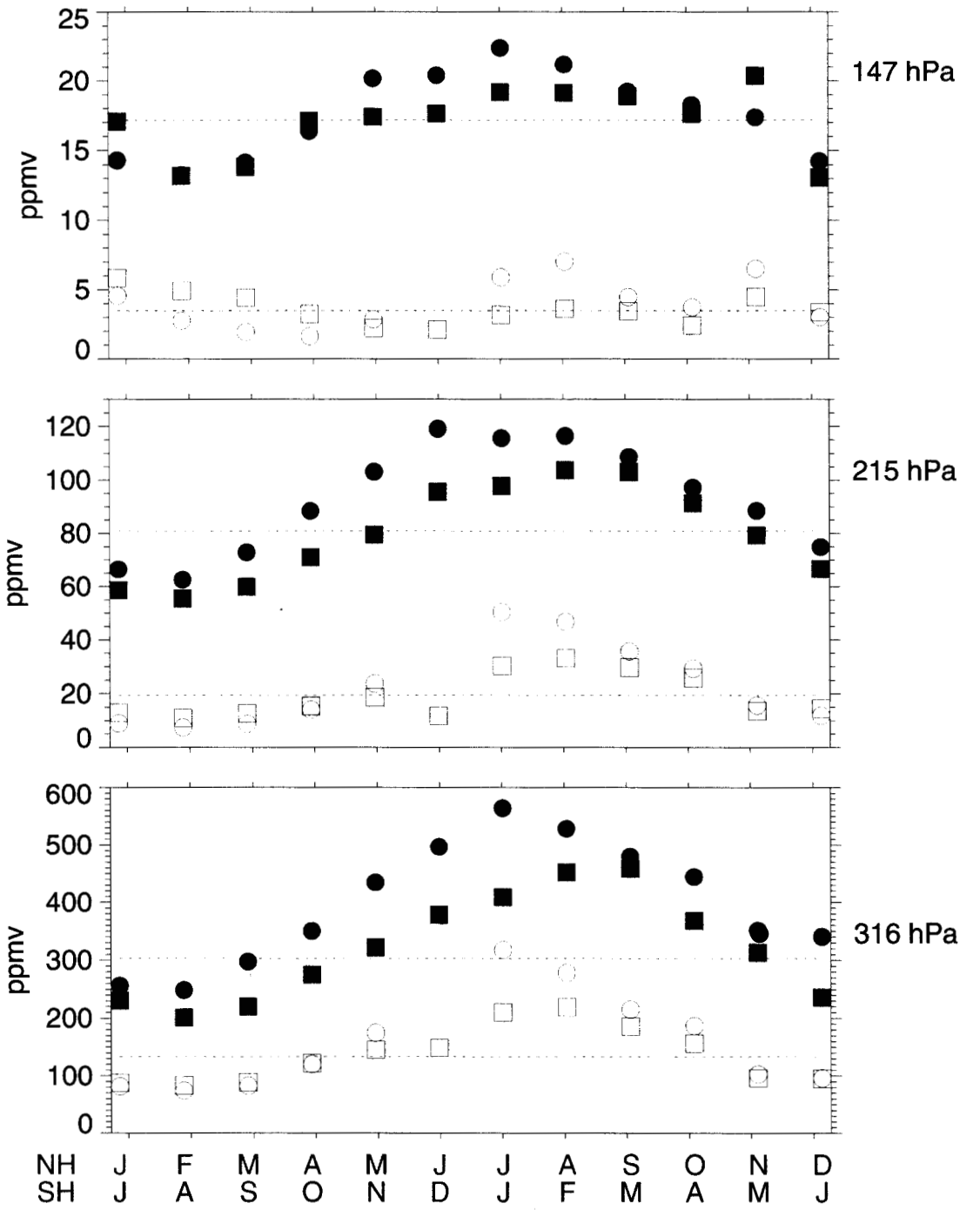

Figure 7. Monthly mean values of MLS upper tropospheric water vapor on the 147, 215, and 316 hPa surfaces. Filled symbols indicate tropical (0°–30° latitude) averages; open symbols indicate extratropical averages (35°–65°). Red (blue) symbols are for SH (NH) data. Dashed lines show the annual averages.

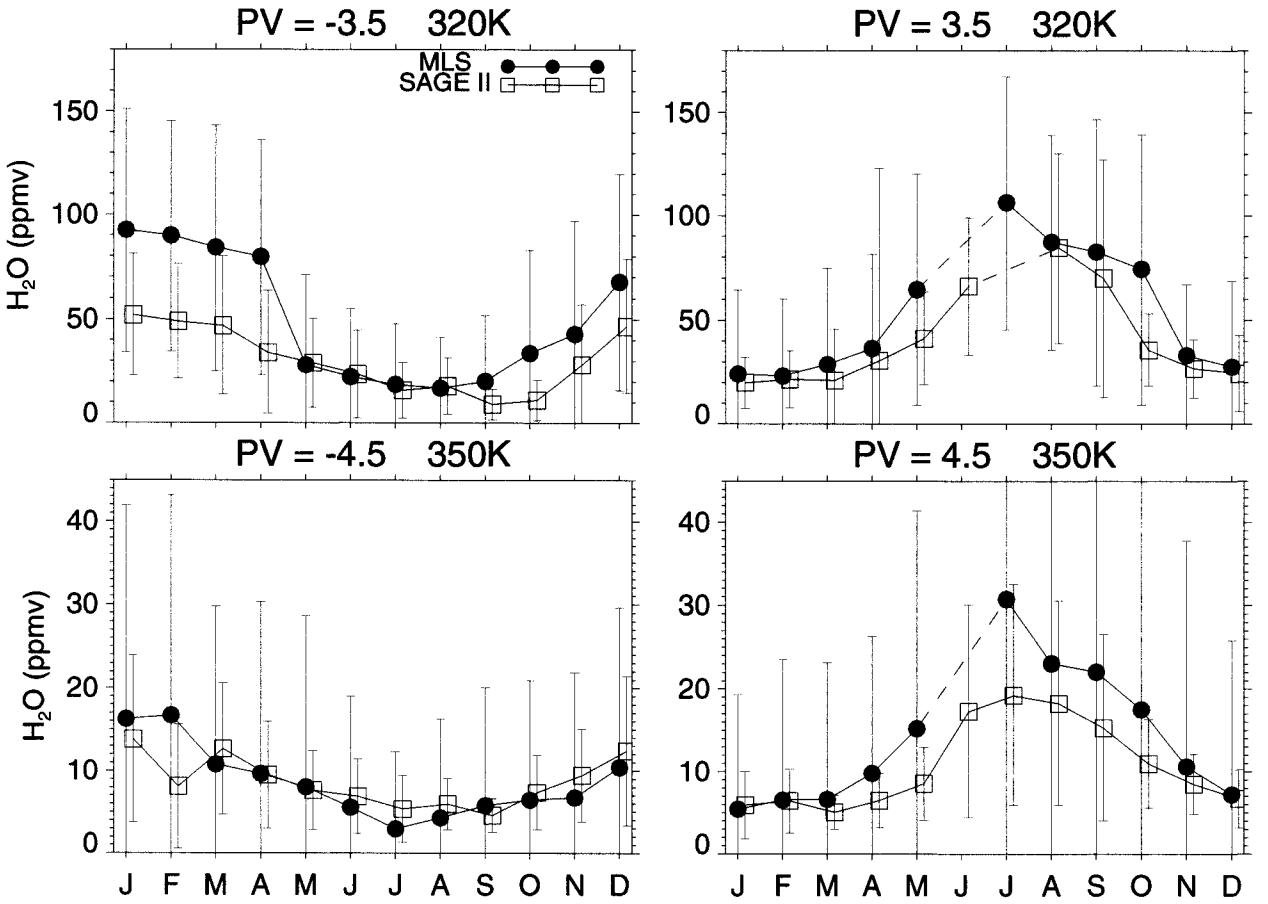

Figure 8. Monthly mean water vapor mixing ratio and rms deviation from MLS (circles) and SAGE II (squares). Data are binned by PV–θ values. Bins sizes are 1 PVU and 10 K. SH means are shown on the left; NH means are on the right.

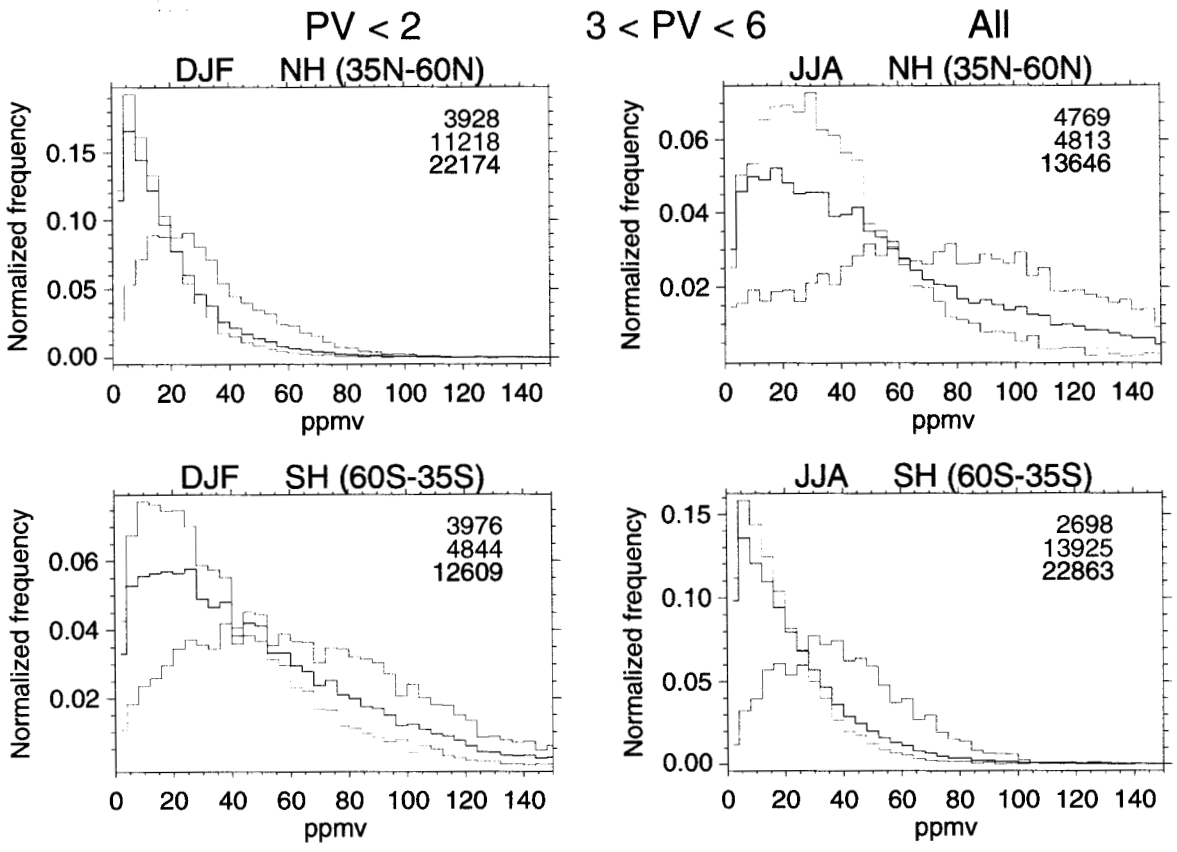

Figure 9. Normalized frequency distributions for midlatitude (35° - 60° latitude) water vapor mixing ratio in the NH and SH for DJF and JJA. Distributions are formed for data with PV $<$ 2 PVU (red), 3 $<$ PV $\leq$ 6 PVU (blue), and all data (black). The number of data points in the distributions is listed in the upper right hand corner each panel.